Skeletal and CNS Defects in *Presenilin-1*-Deficient Mice

Jie Shen,* Roderick T. Bronson,† Dong Feng Chen,*
Weiming Xia,‡ Dennis J. Selkoe,‡
and Susumu Tonegawa*§
*Howard Hughes Medical Institute
Center for Learning and Memory
Center for Cancer Research
Department of Biology
Massachusetts Institute of Technology
Cambridge, Massachusetts 02139
†Department of Pathology
School of Medicine
School of Veterinary Medicine
Tufts University
Boston, Massachusetts 02111
‡Department of Neurology
Center for Neurologic Diseases
Harvard Medical School
Brigham and Women's Hospital
Boston, Massachusetts 02115

Summary

Presenilin-1 (*PS1*) is the major gene responsible for early-onset familial Alzheimer's disease (FAD). To understand the normal function of *PS1*, we have generated a targeted null mutation in the murine homolog of *PS1*. We report that *PS1*$^{-/-}$ mice die shortly after natural birth or Caesarean section. The skeleton of homozygous mutants is grossly deformed. Hemorrhages occur in the CNS of *PS1* null mutants with varying location, severity, and time of onset. The ventricular zone of *PS1*$^{-/-}$ brains is markedly thinner by embryonic day 14.5, indicating an impairment in neurogenesis. Bilateral cerebral cavitation caused by massive neuronal loss in specific subregions of the mutant brain is prominent after embryonic day 16.5. These results show that *PS1* is required for proper formation of the axial skeleton, normal neurogenesis, and neuronal survival.

Introduction

Alzheimer's disease (AD) is the most common cause of dementia in the elderly. The neuropathologic hallmarks of AD include extracellular amyloid plaques, intraneuronal neurofibrillary tangles, and extensive neuronal loss in the cerebral cortex and hippocampus. Early-onset or presenile AD (onset before 65 years) is primarily inherited as autosomal dominant mutations in the amyloid precursor protein gene (*APP*), Presenilin 1 (*PS1*) or Presenilin 2 (*PS2*) genes (Levy-Lahad et al., 1995; Rogaev et al., 1995; Sherrington et al., 1995; Selkoe, 1996). The *PS1* gene harbours an estimated 70% of the pathogenic mutations, making it the major gene involved in early-onset familial AD (FAD). Twenty-five distinct missense

mutations, and a single point mutation at a splice acceptor site resulting in an in-frame deletion of exon 9, have been identified in the *PS1* gene in FAD pedigrees (Campion et al., 1995; Chapman et al., 1995; Cruts et al., 1995; Group, 1995; Perez-Tur et al., 1995; Sherrington et al., 1995; Wasco et al., 1995). PS2 shares 67% amino acid sequence identity with PS1, and two missense mutations in the *PS2* gene have also been identified in early-onset FAD cases (Levy-Lahad et al., 1995; Rogaev et al., 1995).

Since the identification of *PS1*, considerable progress has been made in defining its structure and intracellular localization. PS1 is a transmembrane protein containing between seven and nine transmembrane domains and a hydrophilic loop region (Sherrington et al., 1995; Slunt et al., 1995). Immunocytochemical analysis has shown that PS1 is localized mainly in the endoplasmic reticulum and, to a lesser extent, in the Golgi compartment (Kovacs et al., 1996; Walter et al., 1996). The N-terminal, loop, and C-terminal domains of PS1 are oriented toward the cytoplasm (Doan et al., 1996). PS1 is subject to endoproteolytic cleavage to generate two fragments of approximately 17 and 27 kDa (Thinakaran et al., 1996; Podlisny et al., 1997).

PS1 is broadly expressed in a variety of tissues, including the embryonic and adult brain (Sherrington et al., 1995; Lee et al., 1996; Berezovska et al., 1997). More detailed analysis has demonstrated that *PS1* is primarily expressed in neurons, and its expression is higher in the cerebellum and hippocampal formation than in the cerebral cortex (Kovacs et al., 1996; Lee et al., 1996; Susuki et al., 1996). Interestingly, the level of *PS1* mRNA is significantly higher in the developing mouse brain than in the adult mouse brain (Lee et al., 1996). Although the function of *PS1* remains unknown, clues to its function have come from the identification of its C. elegans homolog, *sel-12*. SEL-12 shares about 50% amino acid sequence identity with PS1, and is a suppressor/enhancer of LIN-12, a member of the LIN-12/Notch family of receptors (Levitan and Greenwald, 1995). *PS1* and *PS2* appear to be functional homologs of *sel-12*, since wild-type *PS1* and *PS2* cDNAs can complement *sel-12* function effectively, whereas the *PS1* and *PS2* cDNAs containing pathogenic mutations show reduced ability to rescue *sel-12* mutations (Levitan et al., 1996). These results suggest that the Presenilins may interact functionally with the Notch signaling pathway. This hypothesis is supported further by the fact that *Notch* and the *presenilins* are coexpressed abundantly in neural progenitor cells within the ventricular zone (Berezovska et al., 1997).

Several lines of evidence have also suggested that the Presenilins may be involved in apoptosis. In one report, a truncated form of murine PS2, ALG-3, was shown to act as a dominant-negative inhibitor of T cell receptor–induced apoptosis in a mouse T cell hybridoma (Vito et al., 1996). In a second study, overexpression of *PS2* was found to increase apoptosis induced by trophic factor withdrawal in PC 12 cells, and a FAD-associated *PS2* mutation could induce apoptosis even

without trophic factor withdrawal (Wolozin et al., 1996). It is possible that FAD-associated mutations increase the susceptibility of neurons to apoptotic stimuli leading to accelerated neuronal death in the brains of AD patients.

To characterize the normal physiological role of *PS1*, we have generated mice with a targeted disruption in the *PS1* locus. We find that homozygous mutant mice derived from four independent embryonic stem (ES) cell lines die minutes after natural birth or C-section with gross skeletal malformation and CNS abnormalities. Histological analysis of the homozygous mutant brains between embryonic day 9.5 and postnatal day 0 reveals that the ventricular zone in the ganglionic eminence is substantially thinner in the mutant brain after embryonic day 14.5, indicating a drastic reduction in the number of neural progenitor cells. Symmetric loss of neural progenitor cells in the ventricular zones of the third and lateral ventricles begins to occur at embryonic days 12.5 and 14.5, respectively. By embryonic day 16.5, bilateral cerebral cavitation caused by massive loss of neural progenitor cells and neurons in the ventrolateral region of the ventricular zone and in the subcortical region of the temporal lobe, respectively, becomes prominent in the mutant brain. These data indicate that *PS1* is required for proper formation of the axial skeleton, and is involved in normal neurogenesis and survival of progenitor cells and neurons in specific brain subregions.

Results

Generation of *PS1* Homozygous Mutant Mice
A genomic library from the 129/Sv mouse strain was screened with a murine *PS1* cDNA fragment spanning exons 1 to 3. Three overlapping genomic clones were isolated, subcloned, and mapped in detail, and the exon–intron boundaries were sequenced. To generate a null mutation in *PS1*, two targeting vectors were constructed, J1.#38 and D3.#37, in which the ATG-containing exon 3 is replaced with a *pgk-neo* cassette (J1.#38 is shown in Figure 1a). Linearized J1.#38 and D3.#37 were then transfected into J1 and D3 ES cells, respectively. A total of 720 G418-resistant ES clones (480 J1 and 240 D3 clones) were screened by Southern analysis for homologous recombination. Correct homologous recombination events were confirmed for one J1 clone and six D3 clones by performing SpeI and BamHI digests followed by hybridization using the 5′ and 3′ genomic probes, respectively (Figures 1b and 1c).

The correct J1 clone and three of the correct D3 clones were microinjected into C57BL/6 mouse blastocysts, and the resulting chimaeras were mated to C57BL/6 mice. Germline transmission was obtained from all four injected ES lines. Offspring from heterozygous intercrosses were typed either by Southern blotting (Figure 1d), or by PCR (Figure 1e) using the primers indicated in Figure 1a. Mating between heterozygous mice yielded the expected Mendelian ratios: 26% of embryos (n = 338), taken between days 16.5 and 18.5, were homozygous mutants. None of the homozygous mutants (n = 92) survived for longer than 30 min after natural birth (n = 4) or C-section (n = 88), but most of them (n = 90)

survived embryonic development in the uterus and were alive at the time of natural delivery or C-section. Only two mutants were found to be dead with severe CNS hemorrhages after C-section at embryonic day 16.5. We therefore conclude that absence of *PS1* leads to neonatal lethality, with rare cases of embryonic lethality caused by extensive CNS hemorrhages.

PS1 Expression in *PS1*$^{-/-}$ Mutants
To determine whether *PS1* is completely inactivated in the homozygous mutants, Northern blot, RT–PCR, and IP–Western analyses were performed. Northern analysis showed that the level of *PS1* mRNA is reduced in heterozygotes compared to wild-type pups (Figure 2a). A residual amount of mutant *PS1* mRNA, which is smaller in size than wild-type *PS1* mRNA, was detected in homozygotes (Figure 2a). RT–PCR was then performed to determine whether this smaller form represents aberrant skipping of exons 2 and 3, which are disrupted in the −/− mutants. A PCR product corresponding to the normal splice form including exons 1 through 5 was found in +/+ pups, whereas aberrant splice forms lacking either exons 2 and 3 or exons 2 through 4 were found in −/− animals (Figure 2b). Since the residual *PS1* mRNA detected in −/− mutants lacks the endogenous ATG codon, it is likely that no endogenous PS1 protein is made in these mutants, though low levels of truncated proteins could conceivably be generated from downstream ATG codons. Since PS1 is normally processed into N-terminal and C-terminal fragments (Thinakaran et al., 1996), and there are in-frame ATG codons in *PS1* exons 4 and 5, we performed IP–Western analysis to test whether the intact C-terminal fragment is present in −/− mutants. A more intense 17 kDa band corresponding to the PS1 C-terminal fragment was found in wild type than that in heterozygotes, whereas no C-terminal fragment was detected in homozygous mutants (Figure 2c). We therefore conclude that the targeted *PS1* mutation is a null allele.

Phenotypic Characterization of *PS1* Mutant Mice
PS1 heterozygous knockout mice are viable and fertile, and indistinguishable from their wild-type littermates by visual inspection. Homozygous mutants derived from all four ES clones are born with tails that are dramatically shortened and curled toward the right side of the body (Figure 3a). These homozygous neonates weigh 15%–20% less than their littermates and have shorter rostrocaudal body axes. They lack the normal cervical and lumbar flexures of the vertebral column and display thickened necks, loose skin, and hindlimbs curved toward the midline. Homozygous mutants also have intracranial hemorrhages with varying degrees of severity. A severe case in which the hemorrhage is visible over most of the head is shown in Figure 3a. The time of onset of hemorrhage varies among embryos and can appear as early as embryonic day 12.5 (Figure 3b). At this stage, the severity of the hemorrhage ranges from the extensive hemorrhage seen in the middle embryo to the very mild form seen in its littermate on the right in Figure 3b. A more consistent aspect of the mutant
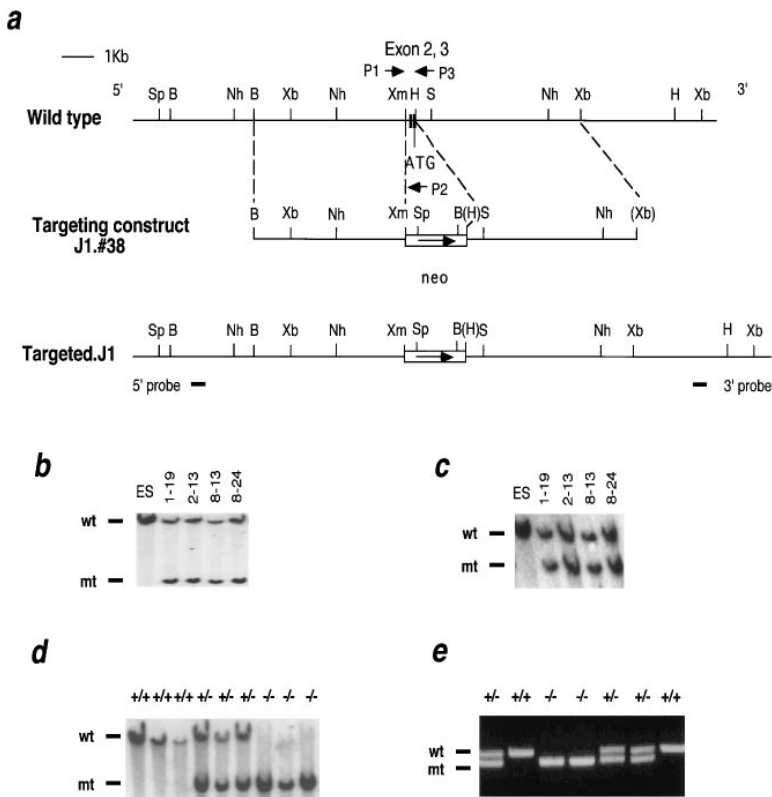
Figure 1. Generation of PS1-Deficient Mice

(a) Schematic representation of the targeting strategy used to disrupt the first coding exon, exon 3 (Sherrington et al., 1995). Black boxes represent *PS1* exons 2 and 3, which are flanked by large introns (>10 kb). The *pgk-neo* cassette is indicated by an open box, and the arrows indicate the direction of transcription. Vertical dashed lines outline the *PS1* genomic sequences incorporated into the targeting construct, J1.#38. About 300 bp of *PS1* genomic DNA (XmaI–HaeII), including exon 2 and most of exon 3, is replaced with the *pgk-neo* cassette in J1.#38, and about 800 bp of *PS1* (XmaI–SacI), including exons 2 and 3, is replaced in D3.#37 (not shown). P1, P2, and P3 are PCR primers used for genotyping. P1 and P3 are specific for *PS1* sequences, and P2 is specific for the *pgk-neo* sequence. 5′ and 3′ probes are 0.5 and 0.7 kb fragments used for screening homologous recombinants, and are located outside of the 5′ and 3′ arms. Abbreviations: SpeI (Sp), BamHI (B), NheI (Nh), XbaI (Xb), XmaI (Xm), HaeII (H), SacI (S).

(b) DNA derived from J1 ES cells (ES), the J1-targeted ES clone (1–19), and the D3-targeted ES clones (2–13, 8–13, and 8–24) was digested with SpeI, and then hybridized with the 5′ probe. The 26 kb and 8 kb fragments correspond to the wild-type and the mutant alleles, respectively.

(c) DNA from control ES cells and the four targeted ES clones indicated was digested with Bam HI, and hybridized with the 3′ probe. The 18 kb and 12 kb bands correspond to the wild-type and the mutant alleles, respectively.

(d) Southern blot analysis of DNA isolated from newborn pups derived from crosses of heterozygous mice. SpeI-digested genomic DNA from wild-type (+/+), heterozygotes (+/−), and homozygous mutants (−/−) was hybridized with the 0.5 kb 5′ probe, giving rise to 26 kb and 8 kb bands for wild-type and mutant alleles, respectively.

(e) Genotype analysis of embryos by PCR using a *PS1* intron 1–specific primer (P1, ACCTCAGCTGTTTGTCCCGG), a neo-specific primer (P2, GCACGAGACTAGTGAGACGTG) and a *PS1* exon 3–specific primer (P3, TCTGGAAGTAGGACAAAGGTG). The upper band (345 bp) is specific for the wild-type *PS1* gene, and the lower band (300 bp) is specific for the mutant allele.

phenotype entails defects in formation of the axial skeleton. At embryonic day 9.5, segmentation is less well-defined in homozygous mutants than in wild-type embryos, particularly in the caudal region indicated by arrows (Figure 3c), and by embryonic day 12.5, all mutants display a kinked, shortened tail (indicated by arrows in Figure 3b).

Malformed Axial Skeleton in *PS1* Null Mutants

The external appearance of *PS1* null mutants indicates that their axial body plan is malformed. To study formation of the axial skeleton further, embryos obtained by C-section on day 19 were stained with alizarin red and alcian blue for bone and cartilage, respectively. The axial skeleton and ribs were found to be severely malformed in *PS1* null mutants (Figure 4a). Although vertebrae in the cervical, thoracic, lumbar, and sacral regions are present in the mutants, they are fused and the vertebral column lacks the normal flexures (Figures 4a and 4b). Caudal to the pelvis, the axial skeletal structure is completely missing in the null mutants (Figure 4a). There are approximately 12 pairs of underossified bones and 3–4 pairs of random ossification centers followed by an unossified and unsegmented cartilaginous mass on the dorsal aspect of the vertebral column in the *PS1* null mutants. A total of approximately 23 segments can be identified in the mutant by the 12 pairs of underossified bones in the dorsolateral areas of the cervical and thoracic regions and approximately 11 random ossification centers in the ventromedial area of the thoracic, lumbar, and sacral regions (Figure 4b). Some of these paired underossified bones in the cervical and thoracic regions are randomly fused in the lateral regions. In addition, *PS1*⁻/⁻ mutants have only approximately 9–11 instead of 13 pairs of ribs with the posterior rib segments missing, and the existing ribs underossified and fused (Figures 4c and 4d). Unlike ribs in wild-type mice, which are attached to the vertebral column by cartilage, the ribs in *PS1* mutants are detached from the vertebral column and are only present in the thoracic region in association with these underossified bones in the vertebral column. The sternum of mutant mice is shorter and thicker relative to wild-type mice, and lacks intersternebral cartilage, by which ribs attach to the sternum. An additional skeletal abnormality present in the mutant is underdevelopment of the occipital bones. The bones of the limbs, pelvis, scapulae, and clavicles are morphologically normal in the *PS1* mutant mice.

The results described above demonstrate that *PS1* is required for skeleton formation. To determine whether the malformation of the axial skeleton is due to defects in somite formation, and whether *PS1* is required for
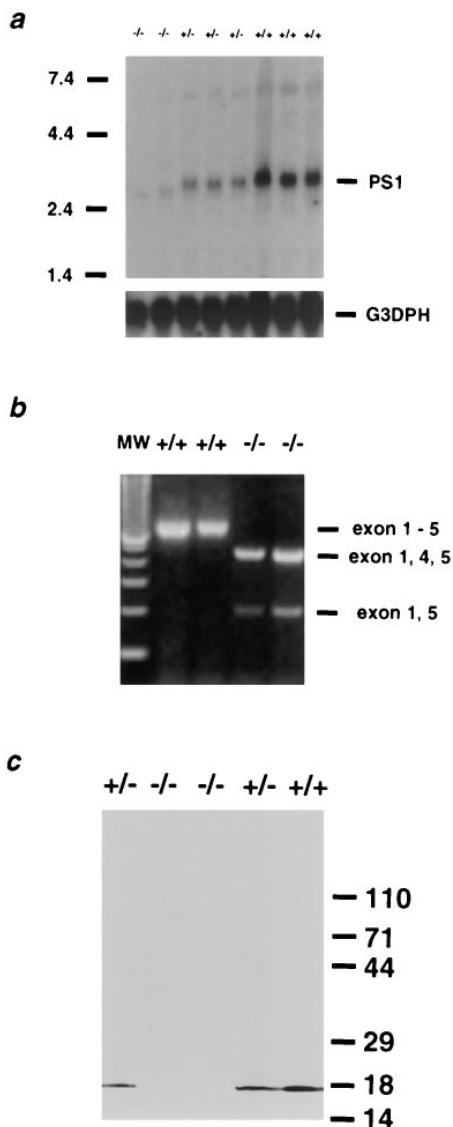
a

b

c

Figure 2. Complete Inactivation of *PS1* Expression in *PS1* Homozygous Mutants

(a) Northern analysis of *PS1* expression. Total RNA was isolated from brains of wild-type, heterozygous and homozygous newborn pups, and hybridized with a 600 bp *PS1* cDNA probe. The *PS1* mRNA band (2.7 kb) was found in +/+ and +/− brains, and a slightly smaller form was found in −/− brains. A very faint 3.4 kb band is present in −/− and +/− lanes, probably derived from aberrant splicing into the *pgk-neo* locus. The same blot was hybridized with a control probe, *G3DPH*, to normalize the amounts of mRNA in each lane.
(b) RT–PCR analysis of *PS1* expression. A primer specific for exon 11 was used for reverse transcription, and primers specific for exons 1 and 5 were used for PCR. An expected 660 bp band was found in wild-type, indicating normal splicing. In −/− mutants, 450 bp and 200 bp products were found, indicating skipping of exons 2 and 3, and of exons 2 through 4, respectively.
(c) IP–Western analysis. A polyclonal antibody raised against the C-terminal 11 amino acid residues of PS1 was used for immunoprecipitation, and a monoclonal antibody raised against the loop region was used as primary antibody for Western blot analysis. A 17 kDa band was found in samples from +/+ and +/− newborn pups, but not from −/− mutants.

normal somitogenesis, day 9.5 and 10.5 embryos were serially sectioned and stained with hematoxylin and eosin. We found that epithelial somites are present in the *PS1* null mutant as in the wild type (Figures 4e and 4f), although the segmentation in the caudal region of *PS1*$^{-/-}$ mice appears less distinct (Figure 3c). In addition, individual compartments of the somites (dermamyotome and sclerotome) are morphologically identifiable in the *PS1*$^{-/-}$ mutants (Figures 4f and 4h). Thus, *PS1* is not required for epithelial somite formation. It is also worth noting that the notochord in the *PS1* null mutant appears to be normal (Figures 4f and 4h), unlike the degenerate notochord in the spontaneous mouse mutant, Danforth's short-tail (*Sd*), which also has a kinky short tail.

Symmetric and Region-Specific Cavitation Caused by Loss of Neural Progenitor Cells and Neurons in *PS1*$^{-/-}$ Brains

PS1 is expressed throughout developing embryos with particularly abundant expression in the ventricular zone of the developing brain (Lee et al., 1996; Berezovska et al., 1997). To identify additional anatomical defects in *PS1* null mutants, day 17.5 embryos were serially sectioned and stained with hemotoxylin and eosin. No gross abnormalities were found in the majority of organs in the homozygous mutants with the exception of lung and brain. The alveoli in the lungs of the null mutant were poorly expanded relative to wild type, probably due to mechanical difficulties imposed by the mutant's defective ribcage. The most striking abnormality observed in the brain consists of symmetric cavitation in the ventrolateral region of the ventricular zone in the posterior portion of the mutant brain (Figures 5b and 5c). As shown in Figures 5a, 5d, and 5g, prominent features of the normal brain at this developmental stage include the ventricular and subventricular zones along the lateral ventricle, the intermediate zone, the subplate, and the developing cortical plate. In addition, the dentate gyrus of the hippocampal formation is becoming a distinct structure at this stage (Figure 5d). In the *PS1* homozygous mutant, the ventricular and subventricular zones in the ventrolateral region are marked by severe loss of neural progenitor cells leading to symmetric cavitation (Figures 5e and 5f). The higher power view of this region shows that the progenitor cells are completely gone and replaced by a cavity (Figures 5h and 5i). Comparison of brain sections from two homozygous mutants (examples shown in Figures 5b and 5c) with brain sections from a heterozygous littermate (an example shown in Figure 5a), which are morphologically indistinguishable from wild-type, reveals symmetric atrophy not only in the ventrolateral region of the ventricular and subventricular zones (indicated by the single arrow in Figures 5e and 5h), but also in the subcortical region of the temporal lobe along the external capsule in the mutant brain (indicated by the double arrow in Figures 5e and 5h). In addition, the lateral ventricles in these homozygous mutants are dilated relative to the control (Figures 5a–5c). In over 40 mutant brains examined at embryonic days 17.5 and 18.5 and the neonatal stage, this striking region-specific and symmetric loss of neurons and neural

Figure 3. Comparison of *PS1* Null Mutants and Their Wild-Type or Heterozygous Littermate Controls at Different Developmental Stages

(a) Lateral view of wild-type and *PS1*-null neonates showing the severely shortened rostrocaudal body axis and tail, as well as intracranial hemorrhage, in the mutant.

(b) Lateral view of heterozygote and null embryos at day 12.5 showing the varying severity of intracranial hemorrhages in the mutants as well as shorter tails in the mutants than in the control (indicated by arrows).

(c) Lateral view of wild-type and null mutant embryos at day 9.5. The arrow indicates the absence of clear segmentation in the caudal region of the mutant.

progenitor cells is always present with varying severity. A consistently associated finding is the thinner cortical plate of the mutant brain relative to that of the control (Figures 5d–5f). The dentate gyrus in PS1−/− mutants is also less distinct at this stage compared to that of the control (Figures 5d–5f).

Another abnormality in the mutant brain is the presence of hemorrhages. As shown previously in Figures 3a and 3b, the *PS1* null mutants have visible intracranial hemorrhages, which occur with varying severity and time of onset. The presence of hemorrhages was carefully examined throughout all serial sections of these two homozygous mutant brains shown in Figure 5. No hemorrhage was found in the midbrain and hindbrain, and a few small, localized hemorrhages were detected in the cerebral cortex of both mutant brains (data not shown). Severe hemorrhages and associated infarcts in the thalamus of one mutant brain are indicated by arrows shown in Figures 5c and 5f, whereas no hemorrhage is seen in the thalamus of the other mutant brain (Figures 5b and 5e). Although the lateral ventricles of the mutant brains are moderately dilated, only trace amounts of blood were detected in the ventricles throughout the brain sections of these two mutants. The cause of hemorrhage is unclear. Examination of the cerebral vasculature in the mutant brain sections revealed no obvious vascular defects (data not shown).

Impaired Neurogenesis in *PS1*−/− Brains

To assess fully the time of onset and progression of the cerebral cavitation occurring in the mutant brain during development, embryos at days 9.5, 10.5, 12.5, 14.5, and 16.5 were serially sectioned and carefully examined for the occurrence of abnormalities in neural development. The presence of hemorrhages was also assessed throughout the brain sections.

Serial sections of six mutant embryos at days 9.5 and 10.5 were compared with their wild-type or heterozygous littermate controls, and no gross abnormalities were found, except that the telencephalic vesicle in the mutants appeared to be smaller, and that mild hemorrhage into the fourth ventricle and the lumen of the neural tube was seen in one of the six mutants (data not shown). Serial transverse sections of three mutant

embryos aged day 12.5 and their littermate controls (+/− or +/+) revealed that the lateral ganglionic eminence is much less prominent in the mutant brains than in the controls (Figures 6a and 6b). There appear to be fewer dividing progenitor cells in the luminal layer of the ventricular zone in the lateral ganglionic eminence in the mutants relative to the controls (Figures 6c and 6d). In addition, the ependymal layer and the ventricular zone at the diencephalic sulcus, which is indicated by the arrows in Figures 6e and 6f, are symmetrically disrupted in the mutants but not in the controls. Two of these three mutant embryos had varying degrees of hemorrhage in the ventricular system.

Similar to the day 12.5 mutant embryos, serial transverse sections of three mutant brains at embryonic day 14.5 show that the lateral ganglionic eminence is less prominent relative to the control (Figures 6g and 6h). The ventricular zone in the *PS1*−/− mutant brains is markedly thinner, indicating a reduction in the number of neural progenitor cells. Although at this embryonic stage the ventricular zone is clearly present in all mutant brain sections examined, disruption of the deepest layers of the ventricular zone, the ependymal and luminal layers, begins to be seen in the ventrolateral region at the posterior portion of the lateral ventricles (indicated by the single arrow in Figure 6j). The mutant brain with the most severe hemorrhage is shown in Figures 6h and 6j, but the symmetric disruption of the ependymal and luminal layers is present in the mutant brains with less or little hemorrhage. At this developmental stage, the hippocampal formation is already quite prominent in the control brain (indicated by the double arrow in Figure 6i) but is hardly recognizable in the mutant brain (indicated by the double arrow in Figure 6j). In addition, the neuronal density along the external capsules appears to be lower in the mutants than in the controls (Figures 6g and 6h). As in day 12.5 mutant embryos, the ventricular zone along the mid-portions of the third ventricle is absent in day 14.5 mutant embryos (data not shown).

More than ten mutant and control embryos aged day 16.5 were serially sectioned, and careful examination of all coronal sections revealed a progression of neuronal loss from anterior to posterior portions of the cerebral hemispheres in the mutants. Comparable coronal sections of the control and mutant brains at three different
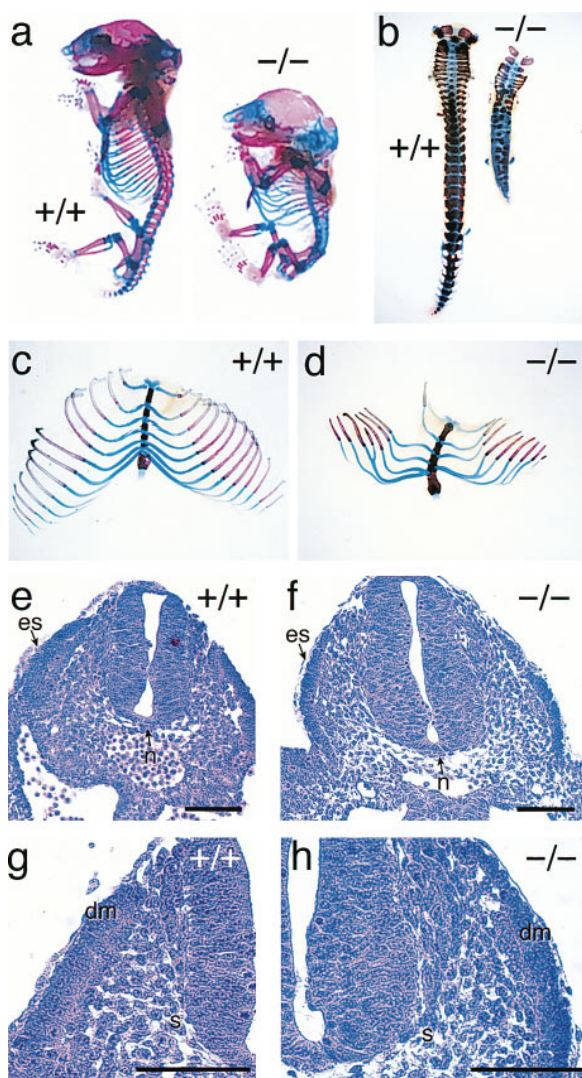
Figure 4. Grossly Defective Axial Skeleton and Morphologically Normal Somites in *PS1*$^{-/-}$ Mice

(a) Lateral view of wild-type and mutant neonates stained for bone (red) and cartilage (blue).

(b) Dorsal view of the dissected vertebral column of wild-type and mutant neonates.

(c and d) Ventral views of the dissected ribcage of wild-type and mutant neonates, respectively.

(e–h) Transverse sections through the hindlimb bud region of day 9.5 wild-type and mutant embryos. Sections were stained with hematoxylin and eosin. Epithelial somites (es) are present in both wild-type (e) and mutant (f) embryos. Under higher magnification, sclerotomes (s) and dermamyotomes (dm) are clearly identifiable in wild-type (g) and mutant (h) embryos. The notochord is indicated as "n" in (e) and (f). Scale bars, 100 μm.

levels are shown in Figures 6k–6s. Comparison of the heterozygote and mutant embryos at an anterior level showed that, consistent with the phenotype observed at earlier developmental stages, the ganglionic eminence is less prominent, and the ventricular zone is thinner in the mutant, though at this level the ependyma is intact (Figures 6k and 6l). At the level of the interventricular foramen of Monroe, where the lateral ventricles join the third ventricle, a more dramatic disruption of

cerebral architecture is evident in the mutant brain, in addition to the thinner ventricular zone and less prominent ganglionic eminence (Figures 6m and 6n). The ependymal and subependymal layers are disrupted in the ventrolateral region but not in the dorsal or ventromedial regions in the mutant brain. The disrupted area in the mutant brain is indicated by the arrow in Figure 6s, and the comparable area in the control is indicated by the arrow in Figure 6r. Bilateral cavitation in the subcortical region of the temporal lobe along the external capsule is already severe in day 16.5 mutant brains (indicated by the single arrow in Figure 6n). The ventricular zone along the lateral portion of the third ventricle is missing in the day 16.5 mutants (indicated by the double arrow in Figure 6n) as in the day 14.5 mutants. At a more posterior level, the day 16.5 mutant brain is similar to the day 17.5 mutant brains shown in Figures 5b and 5c, with severe disruption in the ventrolateral regions of the ventricular zone and in the subcortical region of the temporal lobe along the external capsule (Figure 6q). Careful assessment for the presence of hemorrhages in these brain sections confirmed that the location of hemorrhages appears random and that the severity varies among animals. Hemorrhagic infarcts are sometimes found to be associated with these randomly located hemorrhages.

Discussion

The Cause of Lethality in the *PS1* Null Mutant

To characterize the normal functions of *PS1*, we have generated a null mutation in the *PS1* locus in mice. Homozygous mutant embryos or neonates from four independent ES cell lines all died within minutes after C-section or natural delivery. While observing three female mice giving birth, we found that all four homozygous mutant neonates were born alive, but died shortly thereafter. Among 88 mutants obtained by C-section at embryonic days 16.5 to 18.5, 86 were alive upon C-section, and only 2 were dead with severe intracranial hemorrhages. Most mutant embryos or neonates examined (n > 100) have intracranial hemorrhages with varying degrees of severity. However, the CNS hemorrhages are unlikely to represent the major cause of lethality in the PS1 mutants, since these hemorrhages are in some cases very mild, and are generally insufficient to cause death as a result of brain herniation. Furthermore, hemorrhages rarely involve the vital structures of the hindbrain in the embryos examined between days 16.5 and 18.5. Instead, the cause of lethality is likely to be the marked deformities of the ribcage, which would significantly impair the respiratory mechanics of the mutants. This interpretation is supported by the finding that the lungs of the mutants are incompletely expanded, with hypoinflation of the alveoli evident in cross sections of the lung. This hypothesis is further supported by the finding that another knockout mutant, *paraxis*$^{-/-}$ (Burgess et al., 1996; see detailed discussion below), which has apparently identical ribcage defects but no CNS hemorrhages, also dies shortly after birth, presumably due to respiratory difficulties.
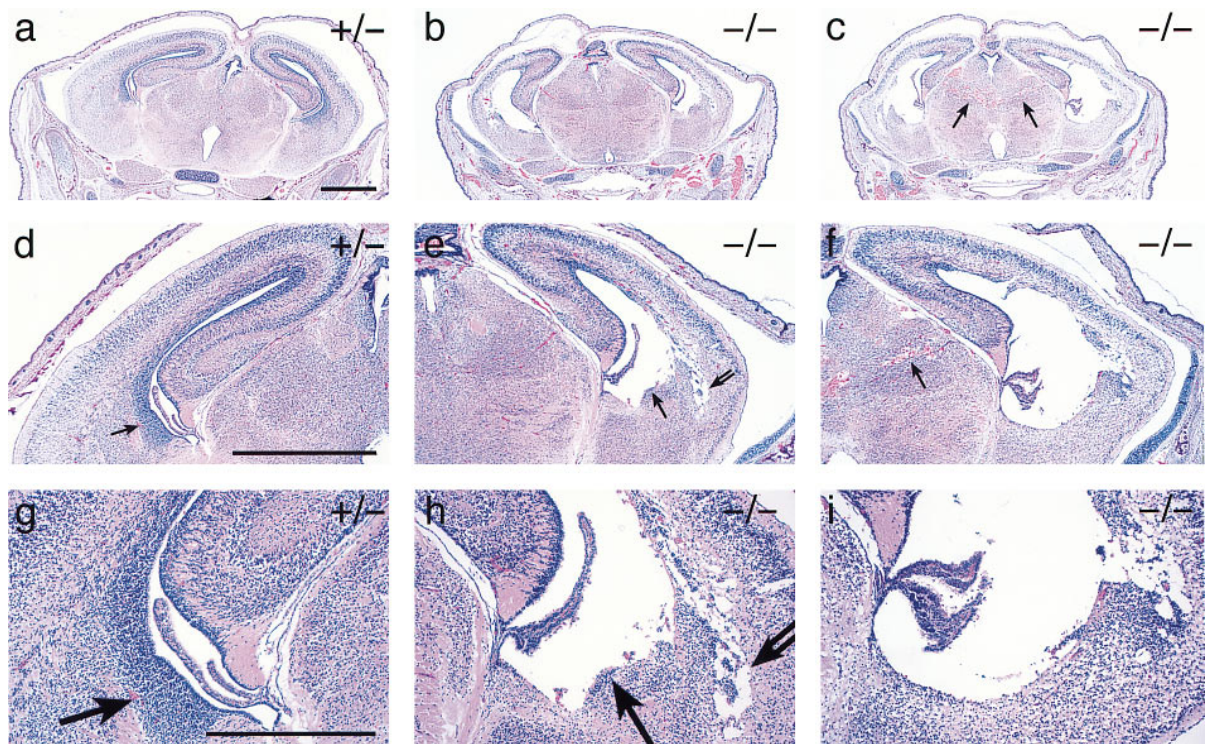
Figure 5. Cerebral Cavitation in Embryonic Day 17.5 Mutant Brains

Heads of a heterozygous control and two homozygous mutants from the same litter were sectioned serially and stained with hematoxylin and eosin. Coronal sections of two independent mutants (b and c) and their littermate control (a) at a comparable level reveal strikingly symmetric cavitation in the posterior portion of the cerebral hemispheres. Under higher magnifications, neural progenitor cells in the ventrolateral region of the ventricular and subventricular zones in these mutants (e, f, h, and i) are completely missing (indicated by the single arrow in [e] and [h]). The subcortical region in the temporal lobe of the mutant brains is disrupted, indicated by the double arrow in [e] and [h]. The cortical plate of the mutant brains is thinner relative to the control (d–f). The arrows in (c) and (f) indicate hemorrhages and associated infarcts in the thalamus. Scale bars, 1 mm in [a] and [d], and 0.5 mm in [g].

The Role of *PS1* in Axial Skeleton Formation

PS1 is essential for proper formation of the axial skeleton, based on the fact that the body axis and skeletal development are disrupted in the *PS1* null mutant. The mechanism by which *PS1* contributes to proper skeleton formation is unclear. Clues to the mechanism have come from studies of other mouse mutants, *Notch1⁻ᐟ⁻* and *paraxis⁻ᐟ⁻*, which display similar skeletal defects and caudal dysgenesis. Notch proteins are a family of cell surface receptors involved in developmental cell fate decisions and lateral inhibition (Artavanis-Tsakonas et al., 1995). At embryonic day 9, the *Notch1* null mutant already displays a deficit in posterior development. Somites in the *Notch1⁻ᐟ⁻* mutant form and subsequently develop into dermamyotome and sclerotome, but the coordination of somite formation is disrupted, leading to variations in somite size and misalignment of the somites across the midline (Conlon et al., 1995; Swiatek et al., 1994). In *PS1⁻ᐟ⁻* mice, epithelial somites as well as the individual somite compartments are clearly present in transverse sections (Figures 4f and 4h). However, as in the case of the *Notch1⁻ᐟ⁻* embryos, the intersomite boundaries are blurred in the caudal region, suggesting a possible interaction of *PS1* with the *Notch* signaling pathway. Such a functional interaction has also been inferred previously from the findings that *PS1* and *Notch*

are coexpressed at high levels in the ventricular zone of the developing mouse brain (Berezovska et al., 1997), and that *PS1* is the functional homolog of *sel-12*, which is a suppressor/enhancer of *lin-12*, a *Notch* family member (Levitan and Greenwald, 1995; Levitan et al., 1996).

Paraxis is a basic helix-loop-helix transcription factor expressed in paraxial mesoderm and somites (Burgess et al., 1995). The external appearance of *paraxis*-null neonates is virtually indistinguishable from the *PS1* null neonates, except that the intracranial hemorrhages often seen in *PS1* mutants are absent in *paraxis* mutants (Burgess et al., 1996). Neonates of both knockouts have dramatically shortened and curled tails. They both lack the normal vertebral flexures and have thickened necks and shortened rostrocaudal body axes. Similar to *PS1* null mutants, the axial skeleton of the *paraxis* null mutants is malformed with fused vertebrae and defective ribcages. The vertebral column of both mutants lacks the normal skeletal and cartilaginous elements of the axial skeleton caudal to the pelvic region. In both mutants, only 20–25 vertebral structure elements in the form of underossified bones and ossification centers can be identified. Ribs of both mutants are underossified and fused and are detached from the vertebral column. Several posterior ribs are missing in both knockouts, and the sterna of both mutants lack intersternebral cartilage,
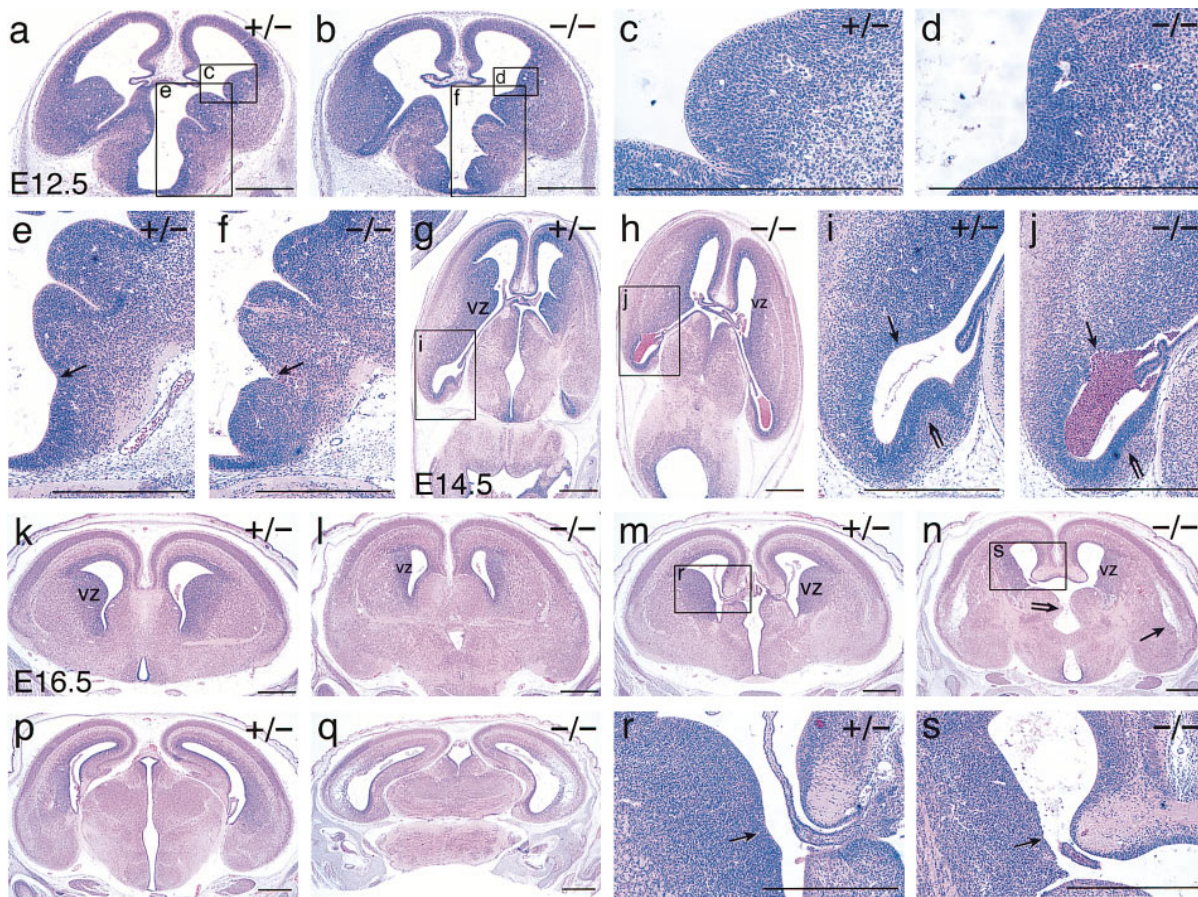
Figure 6. Comparison of the Mutant and Control Brains at Embryonic Days 12.5, 14.5, and 16.5

The scale bars represent 0.5 mm.

(a and b) Transverse brain sections at the level of the interventricular foramen of Monroe (IVF) at embryonic day 12.5. The lateral ganglionic eminence (LGE) is prominent in the heterozygous littermate control (indicated by box [c]) but not in the null mutant (indicated by box [d]). The right halves of the heterozygote and mutant brain sections are most comparable.

(c and d) Higher power views of (a) and (b) in the LGE region showing the difference of LGE in heterozygote and null mutant brains.

(e and f) Higher power views of (a) and (b) in the third ventricle showing the disruption of the ventricular zone in the dorsal diencephalic sulcus, indicated by arrows. The bulge at the top of the panels is the medial ganglionic eminence.

(g and h) Transverse brain sections at the IVF level of the heterozygote and null mutant at embryonic day 14.5. The LGE is prominent in the heterozygote but much less so in the homozygous mutant. The ventricular zone (VZ) is marked thinner in the mutant.

(i and j) Higher power views of (g) and (h) at the posterior portion of the lateral ventricle showing the disruption of the ependymal and luminal layers in the lateral region, which is indicated by the single arrow. The hippocampal formation, indicated by the double arrow, is much less prominent in the mutant.

(k–q) Coronal brain sections of the heterozygote and null mutant at embryonic day 16.5, at an anterior level (k and l), at the IVF level (m and n), and at a more posterior level (p and q). The single arrow in (n) indicates the disruption in the subcortical region of the temporal lobe in the mutant brain, whereas the double arrow indicates the loss of the VZ along the third ventricle.

(r and s) Higher power views of the ganglionic eminence region boxed in (m) and (n). The arrow in (s) indicates the disruption of the ependymal and luminal layers in the ventrolateral region.

through which the ribs attach to the sternum. Although the skeletal phenotypes of the *PS1* and *paraxis* null mutants are indistinguishable, the somitogenesis in the two mutants appears to be different. In *paraxis*$^{-/-}$ mice, cells from the paraxial mesoderm are unable to form epithelial somites, so that all epithelial somites, as well as all morphologically identifiable somite compartments (dermatome, myotome and sclerotome), were absent (Burgess et al., 1996). However, the cells composing the dermatome, myotome, and sclerotome are present in the *paraxis* mutant, as determined by in situ hybridization using the specific probes *Pax-3*, *Pax-7*, and *Pax-9*,

respectively. The striking similarities between the *PS1* and *paraxis* null mutants in skeleton formation and the difference in somite formation suggest that their functions converge in the pathway for skeleton formation. How PS1 and Paraxis interact, the identity of other components of the pathway, and whether Notch1 plays a role in the same pathway remain to be determined.

The Role of PS1 in Neural Development

We have shown a symmetric and region-specific loss of neural progenitor cells and neurons in *PS1*$^{-/-}$ brains (Figures 5 and 6). At embryonic day 12.5, the ventricular

zone of the lateral ventricles is clearly present and intact throughout the mutant brain sections examined (Figures 6b and 6d). At embryonic day 14.5, most layers of the ventricular zone are still clearly present, although it is generally thinner in the mutant brain than in the control (Figures 6h and 6j). However, the deepest layers of the ventricular zone in the ventrolateral region at the posterior portion of the lateral ventricles begin to show signs of degeneration (indicated by the single arrow in Figure 6j). By embryonic day 17.5, all layers of the ventricular zone in the ventrolateral region at the posterior portion of the lateral ventricles are completely gone and replaced by a cavity (Figures 5e, 5f, 5h, and 5i). In addition to this region-specific and progressive degeneration of the ventricular zone, the subcortical region of the temporal lobe also shows substantial degeneration by embryonic day 16.5 (indicated by the single arrow in Figure 6n), whereas at embryonic day 14.5, this subcortical region is still relatively intact (Figure 6h). These results indicate that degeneration of the neural progenitor cells and neurons occurs in a region-specific manner in the ventricular zone and in the subcortical region, respectively. The degeneration of the ventricular zone in the ventrolateral region cannot be explained by reduced proliferation of progenitor cells, and it can only be accounted for by the loss of progenitor cells in this specific region. In addition, reduction in the number of progenitor cells in the ventricular zone cannot explain the degeneration that occurs in the subcortical region of the temporal lobe. How *PS1* protects the neurons and progenitor cells in these specific regions from degeneration during neural development needs to be determined.

In addition to region-specific loss of neural progenitor cells and neurons, neurogenesis is also impaired in *PS1* null mice. Beginning at embryonic day 14.5, the ventricular zone is markedly thinner, indicating a drastic reduction in the number of neural progenitor cells in the mutant (Figures 6g–6s). The most straightforward explanation for the reduced number of progenitor cells is that proliferation is impaired during neurogenesis. This notion is supported by the observation that there appear to be fewer actively dividing progenitor cells in the luminal layer of the ventricular zone in the lateral ganglionic eminence (LGE) of the mutant brain at embryonic day 12.5 (Figure 6d). Previous results have suggested a functional interaction of *PS1* with the *Notch* signaling pathway. *Notch* participates in embryonic neurogenesis in Drosophila, and lack of *Notch* expression leads to a lethal hypertrophy of the nervous system (Artavanis-Tsakonas et al., 1995). Whether *PS1* indeed interacts with *Notch* to effect neurogenesis remains to be resolved. An alternative explanation for the reduction in the number of progenitor cells is increased cell death in the *PS1*⁻/⁻ brain.

Despite the presence of hemorrhages in the mutant brains, the loss of neurons and progenitor cells appears independent of hemorrhages for the following reasons. First, the location of the loss is very symmetric and region-specific, whereas the hemorrhages occur in random locations. Second, the loss of neurons and progenitor cells is a gradual process with increasing severity paralleling the progression of neural development, whereas the severity of hemorrhages and their times of onset are random and independent of the stage of embryonic development. Hemorrhages are sometimes very severe at an early embryonic stage, and conversely, sometimes very mild even at the postnatal stage. Third, severe neuronal loss in some cases occurs in the absence of severe hemorrhage and lateral ventricular dilation, such as in the examples in Figures 5b and 5c. Careful examination of serial sections throughout these two mutant brains showed that there are only trace amounts of blood in the lateral ventricles of both mutants, very mild hemorrhage in the cortex and thalamus of one mutant, and severe and no hemorrhage in the thalamus and cortex of the other mutant, respectively. However, the extent of neuronal loss in these two littermate mutants is very similar (Figures 5b, 5c, 5e, 5f, 5h, and 5i). Although the lateral ventricles are dilated in these two mutant brains, the ventricular system often appears normal in other mutant brains with severe neuronal loss (Figure 6 and data not shown). Given all the reasons listed above, we think it is highly unlikely that the neuronal loss is caused by the hemorrhages. This issue could be addressed more definitively by an in vitro culture of brain slices derived from *PS1* null mutants, or by a conditional *PS1* knockout mouse in which *PS1* expression is disrupted only in neurons during development.

Implications for the Pathogenesis of Alzheimer's Disease

The mechanism by which the pathogenic *PS1* mutations cause AD is still unclear. The pathogenesis could be associated with either a gain of function or a loss of function in *PS1* mutant alleles. The fact that all 26 dominant, fully penetrant mutations in *PS1* are missense mutations, rather than nonsense or frameshift mutations, argues for the former possibility. Further support for this hypothesis has come from the findings that Ab1–42 secretion is increased in FAD patients bearing mutant *PS1* alleles, as well as in transgenic mice and transfected cells overexpressing mutant *PS1* alleles (Borchelt et al., 1996; Duff et al., 1996; Citron et al., 1997; Lemere et al., 1996; Scheuner et al., 1996; Xia et al., 1997). However, it remains possible that the pathogenic mutations lead to a loss of function by lowering the dosage of *PS1* below a critical level (haploinsufficiency). In C. elegans, introduction of several FAD-associated mutant *PS1* cDNAs resulted in only a partial rescue of the *sel-12* mutant phenotype, whereas introduction of the wild-type *PS1* cDNA gave rise to a complete rescue (Levitan et al., 1996; Baumeister et al., 1997). This result suggests that the FAD-associated *PS1* mutations may lead to a reduction in PS1 activity. If this is the case, our finding that lack of *PS1* leads to loss of neural progenitor cells and neurons during development may be relevant to the neuronal loss seen in FAD patients. Although absence of *PS1* expression in mice results in severe developmental defects, it is possible that inactivation of only one *PS1* allele by FAD-associated mutations permits normal development, but has a deleterious effect on neuronal survival in the adult brain. In this respect, it will be interesting to see whether aged heterozygous knockout mice develop AD-like neuropathological defects. Regardless

of whether a gain of function or loss of function is operative in FAD patients, it would be highly useful to generate mice in which FAD-associated mutations have been "knocked-in" to the *PS1* locus. In contrast to transgenic mice overexpressing mutant *PS1* ectopically, such an animal might provide a more natural model for FAD, permitting a more accurate assessment of the effects of pathogenic mutations.

Experimental Procedures

PS1 Targeting Construct
The mouse *PS1* cDNA sequence obtained from GenBank was used to design primers (P5, GGCAGCTGAGGCGGAAACCTAGG and P6, GGATGGCGCTGCTGGAGTGG), which were used to generate a 250 bp cDNA fragment from a mouse brain cDNA library by PCR. This 250 bp fragment, containing sequence corresponding to *PS1* exons 1 to 3, was then used as a probe to screen a 129/Sv genomic phage library. Multiple clones containing overlapping *PS1* genomic regions were identified, subcloned, and carefully restriction mapped. A 5 kb BamHI–XmaI fragment was used as the 5′ arm in both targeting constructs. HaeII–XbaI (5.5 kb) and SacI–NheI (4 kb) fragments were used as the 3′ arms in J1.#38 and D3.#37, respectively. In both constructs, *PS1* exons 2 and 3 are replaced with a 1.8 kb *pgk-neo* cassette.

Detection of Homologous Recombination in ES Cells and Generation of *PS1*-Deficient Mice
ES cells derived from 129/Sv mice were grown on mitotically-inactivated embryonic fibroblast feeder cells and electroporated with 40 μg of the linearized targeting constructs using a Bio-Rad Gene Pulser at 800 V and 3 μF settings. G418 was applied at 200 μg/ml 24 hr later to select for transfectants, and G418-resistant colonies were isolated on days 6 and 7 of selection. Genomic DNA from 720 ES clones was digested with SpeI, and then hybridized with the 5′ external probe (a 0.5 kb HindIII fragment). Among 11 clones that tested positive for homologous recombination at the 5′ arm region, only 7 were confirmed by Bam HI digests followed by hybridization using the 3′ external genomic probe (a 0.7 kb Pst fragment). Four clones (J1.1–19, D3.2–13, D3.8–13, and D3.8–24) were microinjected into C57BL/6 mouse blastocysts, and the resulting chimeras mated to C57BL/6 mice. Germline transmission was obtained from all four injected ES clones.

Northern Analysis and Reverse Transcription–Linked PCR
Total RNA was isolated from brains of newborn pups using the TRI reagent kit from the Molecular Research Center, Inc. Approximately 20 μg RNA of each sample was used for Northern analysis, performed according to Sambrook et al. (1989). The blot was hybridized with a 600 bp *PS1* cDNA probe. The same blot was then hybridized with a human *G3DPH* probe to normalize the amounts of mRNA. Reverse transcription was carried out using M-MuLV reverse transcriptase (BRL) with a *PS1* exon 11-specific primer (P16, TCAGTATG GCTACAAAGCAGG) according to the manufacturer's instructions, except that 15 pmol primer and 100 U reverse transcriptase were used per 20 μl reaction. 1/20 of the reverse transcription product (1 μl) was used for PCR with primers specific for *PS1* exon 1 (P5) and exon 5 (P18, GACCTTGTAGCACCTGTATTTATACAG).

Immunoprecipitation–Western Blot Analysis
Individual mouse brains were weighed and then homogenized in modified STEN-lysis-CHAP buffer at a ratio of 0.1 g brain tissue per ml buffer. The buffer contains 50 mM Tris (pH 7.6), 150 mM NaCl, 2 mM EDTA, 1% NP-40, 12 mM CHAPS {3-[(3 -chloroamidopropyl)-dimethylammonio]-1-propanesulfonate; Pierce), and a protease inhibitor cocktail (5 μg/ml leupeptin, 5 μg/ml aprotinin, 2 μg/ml pepstatin A, and 0.25 mM phenylmethylsulfonl fluoride; Sigma). Lysate was precleared with protein A–Sepharose and preimmune serum for 2 hr and centrifuged for 5 min at 6000 × g. The supernatant derived from the equivalent of 2 mg brain tissue was immunoprecipitated with the polyclonal antiserum 4627 IgG, which was raised against the PS1 synthetic peptide 457–467 (Citron et al., 1997), and covalently linked to protein A–Sepharose (Podlisny et al., 1997). The immunoprecipitated samples were washed with monoclonal antibody 13A11, which was raised against residue 294–309 of PS1 (Podlisny et al., 1997), eluted, and electrophoresed on 8%–16% SDS–polyacrylamide gels and then immunoblotted.

Skeletal Preparation
C-sectioned embryos from approximately embryonic day 19 were eviscerated and skinned, and the skin was used for genotyping. The carcasses were placed in water overnight, then placed in water at 65°C for 1 min and transferred to 100% ethanol for 3 days. The carcasses were then stained with alcian blue (15 mg alcian blue in 80 ml of 95% ethanol and 20 ml of glacial acetic acid) for 12 hr, rinsed in 100% ethanol overnight, cleared in 2% KOH for 6 hr, stained with alizuine red (5 mg in 100 ml of 2% KOH) for 3 hr, and finally cleared again in 2% KOH for 12 hr.

Histology
Embryos were fixed in Bouin's solution or 4% paraformaldehyde and then embedded in paraffin wax. Serial sections of 5 μm were prepared and stained with hematoxylin and eosin.

References

Artavanis-Tsakonas, S., Matsuno, K., and Fortini, M. (1995). Notch signaling. Science *268*, 225–232.

Baumeister, R., Leimer, U., Zweckbronner, I., Jakubek, C., Gruenberg, J., and Haass, C. (1997). The sel-12 mutant phenotype of C. elegans is rescued independent of proteolytic processing by wt but not mutant Presenilin. Genes and Function, in press.

Berezovska, O., Xia, M., Page, K., Wasco, W., Tanzi, R., and Hyman, B. (1997). Developmental regulation of presenilin mRNA expression parallels Notch expression. J. Neuropath. Exp. Neurol. *56*, 40–44.

Borchelt, D.R., Thinakaran, G., Eckman, C.B., Lee, M.K., Davenport, F., Ratovitsky, T., Prada, C., Kim, G., Seekins, S., Yager, D., et al. (1996). Familial Alzheimer's disease-linked presenilin 1 variants elevate Ab1–42/1–40 ratio in vitro and in vivo. Neuron *17*, 1005–1013.

Burgess, R., Cserjesi, P., Ligon, K.L., and Olson, E.N. (1995). Paraxis: a basic helix-loop-helix protein expressed in paraxial mesoderm and developing somites. Dev. Biol. *168*, 296–306.

Burgess, R., Rawls, A., Brown, D., Bradley, A., and Olson, E.N. (1996). Requirement of the paraxis gene for somite formation and musculoskeletal patterning. Nature *384*, 570–573.

Campion, D., Flaman, J.M., Brice, A., Hannequin, D., Dubois, B., Martin, C., Moreau, V., Charbonnier, F., Didierjean, O., Tardieu, S., et al. (1995). Mutations of the presenilin 1 gene in families with early-onset Alzheimer's disease. Hum. Mol. Genet. *4*, 2373–2377.

Chapman, J., Asherov, A., Wang, N., Treves, T.A., Korczyn, A.D., and Goldfarb, L.G. (1995). Familial Alzheimer's disease associated with S182 codon 286 mutation. Lancet *346*, 1040.

Citron, M., Westaway, D., Xia, W., Carlson, G., Diehl, T., Levesque, G., Johnson-Wood, K., Lee, M., Seubert, P., Davis, A., et al. (1997). Mutant presenilins of Alzheimer's disease increase production of 42-residue amyloid β-protein in both transfected cells and transgenic mice. Nature Med. *3*, 67–72.

Conlon, R.A., Reaume, A.G., and Rossant, J. (1995). Notch 1 is required for the coordinate segmentation of somites. Development *121*, 1533–1545.

Cruts, M., Backhovens, H., Wang, S.Y., Vangassen, G., Theuns, J., Dejonghe, C., Wehnert, A., Devoecht, J., deWinter, G., Cras, P., et al. (1995). Molecular genetic analysis of familial early-onset Alzheimer's disease linked to chromosome 14Q24.3. Hum. Mol. Genet. *4*, 2363–2371.

Doan, A., Thinakaran, G., Borchelt, D.R., Slunt, H.H., Ratovitsky, T., Podlisny, M., Selkoe, D.J., Seeger, M., Gandy, S.E., Price, D.L., and Sisodia, S.S. (1996). Protein topology of presenilin 1. Neuron *17*, 1023–1030.

Duff, K., Eckman, C., Zehr, C., Yu, X., Prada, C., Perez-tur, J., Hutton, M., Buee, L., Harigaya, Y., Yager, D., et al. (1996). Increased amyloid-β42(43) in brains of mice expressing mutant presenilin 1. Nature *383*, 710–713.

Group, Alzheimer's Disease Collaborative (1995). The structure of the presenilin 1 (S182) gene and identification of six novel mutations in early onset AD families. Nature Genet. *11*, 219–222.

Kovacs, D.M., Fausett, H.J., Page, K.J., Kim, T.-W., Moir, R.D., Merriam, D.E., Hollister, R.D., Hallmark, O.G., Mancini, R., Felsenstein, K.M., et al. (1996). Alzheimer-associated presenilins 1 and 2: neuronal expression in brain and localization to intracellular membranes in mammalian cells. Nature Med. *2*, 224–229.

Lee, M.K., Slunt, H.H., Martin, L.J., Thinakaran, G., Kim, G., Gandy, S.E., Seeger, M., Koo, E., Price, D.L., and Sisodia, S.S. (1996). Expression of presenlin 1 and 2 (PS1 and PS2) in human and murine tissues. J. Neurosci. *16*, 7513–7525.

Lemere, C.A., Lopera, F., Kosik, K.S., Lendon, C.L., Ossa, J., Saido, T.C., Yamaguchi, H., Ruiz, A., Martinez, A., Madrigal, L., et al. (1996). The E280A presenilin 1 mutation leads to a distinct Alzheimer's disease phenotype: increased Aβ42 deposition and severe cerebellar pathology. Nature Med. *2*, 1146–1150.

Levitan, D., and Greenwald, I. (1995). Facilitation of lin-12-mediated signaling by sel-12, a *Caenorhabditis elegans* S182 Alzheimer's disease gene. Nature *377*, 351–354.

Levitan, D., Doyle, T.G., Brousseau, D., Lee, M.K., Thinakaran, G., Slunt, H.H., Sisodia, S.S., and Greenwald, I. (1996). Assessment of normal and mutant human presenilin function in *Caenorhabditis elegans*. Proc. Natl. Acad. Sci. USA *93*, 14940–14944.

Levy-Lahad, E., Wasco, W., Poorkaj, P., Romano, D.M., Oshima, J., Pettingell, H., Yu, C., Jondro, P.D., Schmidt, S.D., Wang, K., et al. (1995). Candidate gene for the chromosome 1 familial Alzheimer's disease locus. Science *269*, 973–977.

Perez-Tur, J., Froelich, S., Prihar, G., Crook, R., Baker, M., Duff, K., Wragg, M., Busfield, F., Lendon, C., Clark, R.F., et al. (1995). A mutation in Alzheimer's disease destroying a splice acceptor site in the presenilin-1 gene. Neuroreport *7*, 297–301.

Podlisny, M.B., Citron, M., Amarante, P., Sherrinton, R., Xia, W., Zhang, J., Diehl, T., Levesque, G., Fraser, P., Haass, C., et al. (1997). Presenilin proteins undergo heterogeneous endoproteolysis between Thr$_{291}$ and Ala$_{299}$ and occur as stable N- and C-terminal fragments in normal and Alzheimer brain tissue. Neurobiol. Dis. *3*, 325–333.

Rogaev, E.I., Sherrington, R., Rogaeva, E.A., Levesque, G., Ikeda, M., Liang, Y., Chi, H., Lin, C., Holamn, K., Tsuda, T., et al. (1995). Familial Alzheimer's disease in kindreds with missense mutations in a gene on chromosome 1 related to the Alzheimer's disease type 3 gene. Nature *376*, 775–778.

Sambrook, J., Fritsch, E.F., and Maniatis, T. (1989). Molecular Cloning, a Laboratory Manual. 2nd Ed. (New York: Cold Spring Harbor Labroratory Press).

Scheuner, D., Eckman, C., Jensen, M., Song, X., Citron, M., Suzuki, N., Bird, T.D., Hardy, J., Hutton, M., Kukull, W., et al. (1996). Secreted amyloid β protein similar to that in the senile plaques of Alzheimer's disease is increased in vivo by the presenilin 1 and 2 and *APP* mutations linked to familial Alzheimer's disease. Nature Med. *2*, 864–870.

Selkoe, D.J. (1996). Amyloid β-protein and the genetics of Alzheimer's disease. J. Biol. Chem. *271*, 18295–18298.

Sherrington, R., Rogaev, E.I., Liang, Y., Rogaeva, E.A., Levesque, G., Ikeda, M., Chi, H., Lin, C., Li, G., Holman, K., et al. (1995). Cloning of a novel gene bearing missense mutations in early onset familial Alzheimer disease. Nature *375*, 754–760.

Slunt, H.H., Thinakaran, G., Lee, M.K., and Sisodia, S.S. (1995). Nucleotide sequence of the chromosome 14-encoded S182 cDNA and revised secondary structure prediction. Int. J. Exp. Clin. Invest. *2*, 188–190.

Susuki, T., Nishiyama, K., Murayama, S., Yamamoto, A., Sato, S., Kanazawa, I., and Sakaki, Y. (1996). Regional and cellular presenilin1 gene experssion in human and rat tissues. Biochem. Biophys. Res. Commun. *219*, 708–713.

Swiatek, P.J., Lindsell, C.E., Franco del Amo, F., Weinmaster, G., and Gridley, T. (1994). Notch 1 is essential for postimplantation development in mice. Genes Dev. *8*, 707–719.

Thinakaran, G., Borchelt, D.R., Lee, M.K., Slunt, H.H., Spitzer, L., Kim, G., Rotovitsky, T., Davenport, F., Nordstedt, C., Seeger, M., et al. (1996). Endoproteolysis of presenilin 1 and accumulation of processed derivatives in vivo. Neuron *17*, 181–190.

Vito, P., Lacana, E., and D'Adamio, L. (1996). Interfering with apoptosis: Ca^{2+} binding protein ALG-2 and Alzheimer's disease gene ALG-3. Science *271*, 521–525.

Walter, J., Capell, A., Grunberg, J., Pesold, B., Schindzielorz, A., Prior, R., Podlisny, M.B., Fraser, P., St. George Hyslop, P., Selkoe, D.J., and Haass, C. (1996). The Alzheimer's disease-associated presenilins are differentially phosphorylated proteins located predominantly within the endoplasmic reticulum. Mol. Med. *2*, 673–691.

Wasco, W., Pettingell, W.P., Jondro, P.D., Schmidt, S.D., Gurubhagavatula, S., Rodes, L., DiBlasi, T., Romano, D.M., Guenette, S.Y., Kovacs, D.M., Growdon, J.H., and Tanzi, R.E. (1995). Familial Alzheimer's chromosome 14 mutations. Nature Med. *1*, 848.

Wolozin, B., Iwasaki, K., Vito, P., Ganjei, J.K., Lacana, E., Sunderland, T., Zhao, B., Kusiak, J.W., Wasco, W., and D'Adamio, L. (1996). Participation of presenilin 2 in apoptosis: enhanced basal activity conferred by an Alzheimer mutation. Science *274*, 1710–1713.

Xia, W., Zhang, J., Kholodendo, D., Citron, M., Podlisny, M.B., Teplow, D.B., Haass, C., Seubert, P., Koo, E.H., and Selkow, D.J. (1997). Enhanced production and oligomerization of the 42-residue amyloid β-protein by Chinese hamster ovary cells stably expressing mutant presenilins. J. Biol. Chem. *272*, 7977–7982.